Pergamon

Int. J. Heat Mass Transfer. Vol. 39, No. 15, pp. 3139–3145, 1996

0017–9310/96 $15.00 + 0.00

PII: S0017-9310(96)00002-6

Heat transfer regime map for electronic devices cooling

KAZUYOSHI FUSHINOBU,† KUNIO HIJIKATA and YASUO KUROSAKI
Faculty of Engineering, Tokyo Institute of Technology, Meguro-ku, Tokyo 152, Japan

(*Received* 30 *August* 1995 *and in final form* 8 *December* 1995)

Abstract—A simple analytical model that predicts the temperature rise of a small heater on an unheated substrate is presented. The model approximates uniform temperature over both the heater and the substrate, although they have spatial distributions in actual case. A rigorous numerical calculation has been performed to verify the model results. A regime map is constructed based on the analytical model. Each regime in the map is named in order to show the time dependency and the governing heat transfer mode of the heater temperature rise. Copyright © 1996 Elsevier Science Ltd.

INTRODUCTION

Background

Due to the continuous miniaturization of electronic devices, the thermal design of these devices is becoming more and more important. Since the purpose of the thermal design is to predict or to control equipment reliability, the temperatures of heat generating components where device failure occurs must be known. Significant progress in the thermal issues of electronic equipment has been made so far. However, most of the works are aimed at specific applications or geometries, hence they cannot be applied to general kinds of problems. A new model that yields more general heat transfer characteristics is therefore needed.

The heat transfer problem in electronic equipment can be modeled as an array of heat generating components (heater) mounted on a nonheating substrate and exposed to a moving cooling fluid. The heater has, in general, two heat transfer paths: direct heat transfer from the heater to the fluid and heat conduction through the substrate, followed by heat transfer from the substrate to the fluid. It is therefore a conjugate heat transfer problem and both mechanisms must be accounted for in a heat transfer model.

Previous works

Although several studies considered the conjugate nature of the electronic components cooling [1, 2], self heating effect of each device was first presented by Hijikata *et al.* [3], who analyzed the heat transfer characteristics from electrically heated diode elements in an IC chip. In this work, the plastic cover of the IC chip was removed to directly expose the internal diode elements to the air impingement cooling. The temperature of each diode element was measured to be much higher than that of the chip bulk value. It was suggested that the chip bulk temperature rise is determined by the total heating rate that is given by the summation of the heat generation rate of each diode in the chip. However, it was also suggested that the local temperature rise, which is defined to be the temperature difference of each diode element and the chip bulk, is proportional to the heating rate of each diode.

Due to the lack of the rigorous numerical approach to the problem, Nagasaki *et al.* [4] performed a three-dimensional steady-state numerical calculation of forced convection heat transfer from a small heater on a substrate. The conclusions of their work emphasized the difference of the governing heat transfer mode at different length scales; although the substrate temperature is governed by the convection, the heater temperature rise is mainly determined by the conduction heat transfer in the substrate.

Due to the periodic nature of the electrical heating in many applications, Fushinobu *et al.* [5] proposed a three-dimensional, periodic steady-state numerical calculation of the temperature rise of the small heater on a substrate using a domain decomposition technique. They concluded that the calculated results show a good agreement with previous experiments. A rigorous tool to predict the temperature rise of the small heaters was developed that revealed the basic heat transfer characteristics. However, a simple predictive procedure for the heater temperature incorporating the obtained heat transfer characteristics has not yet been proposed. Since the engineering applications require simple and general temperature prediction tools, development of a new model is desired.

Objectives

This work develops a new, simple, and easy to use analytical model that predicts the general behavior of

† Address: Department of Mechanical and Intelligent Systems Engineering, Tokyo Institute of Technology, Meguro-ku, Tokyo 152, Japan.

NOMENCLATURE

Bi	Biot number
Fo	Fourier number
f	heating frequency [Hz]
i	imaginary unit $= \sqrt{-1}$
L_e	heater size [m]
L_s	substrate length [m]
L_y	substrate thickness [m]
Q	amplitude of periodic heat generation rate in a heater [W]
Re	Reynolds number
T	temperature [K]
t	time [s].

Greek symbols

α	thermal diffusivity [$m^2\ s^{-1}$]
γ_e	heater-substrate size ratio $\equiv L_e/L_s$
γ_s	substrate thickness-length ratio $\equiv L_y/L_s$
λ	thermal conductivity [W (m-K)$^{-1}$]
θ	nondimensional temperature rise
τ	nondimensional time.

Subscripts

c	conduction governed heater local value
co	conduction governed heater local value at $f/f_e = 0$
e	heater
f	fluid
s	substrate or convection governed substrate value
so	convection governed substrate value at $f/f_e = 0$.

the temperature rise of a small heater mounted on an unheated substrate and cooled by a surrounding fluid. The model simulates the operating electronic devices in an integrated circuit chip. The boundary layer flow on a flat plate models the convective cooling. Furthermore, the velocity boundary layer starts before the thermal boundary layer, which appears most applications. A sinusoidal time-dependent heat generation is considered in the heater. Since the maximum device temperature rise is the major concern during device operation, only the amplitude of the heater temperature rise is discussed. The model results are compared with the results of rigorous three-dimensional, periodic steady-state numerical computations. Finally, the model results are used to construct a regime map that indicates the heat transfer characteristics based on heater size and heating time.

ANALYTICAL MODEL

Modeling of the temperature rise

The numerical and experimental results [3, 4] suggest that although the substrate temperature rise is influenced by the fluid flow, the heater local temperature rise, which is defined as the temperature difference between the heater and the bulk substrate, is mainly governed by the heat conduction in the vicinity of the heater. The analytical model developed here thus assumes the heater temperature rise to be a combination of the conduction-governed heater temperature rise and the convection-governed substrate temperature rise. Figure 1 shows a schematic of the modeling of the temperature field. Uniform temperature increases in the heater and substrate temperatures approximate the actual temperature distribution. The heater temperature rise, ΔT_e, is given as a summation of the conduction-governed local heater temperature rise, ΔT_c, and the convection-governed substrate temperature rise, ΔT_s. Note that ΔT_e, ΔT_c and ΔT_s are the amplitudes of time-dependent fluctuation of the temperatures

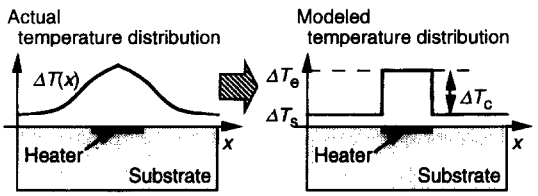

Fig. 1. A schematic depicting the modeling of the substrate temperature distribution. The model approximates the uniform temperature rise of both the heater and the substrate.

Conduction-governed heater local temperature rise

Amplitude of the conduction-governed local heater temperature rise, ΔT_c, is determined from the periodic steady-state one-dimensional heat conduction solution of a hemispherical heater in a semi-infinite medium [6],

$$\Delta T_c = AQ(2\pi\lambda_s^2 L_e^2)^{-1/2}\{(1+\sqrt{t_e f})^2 + t_e f\}^{-1/2}, \quad (1)$$

where $A = 1$, Q is the amplitude of the heat generation rate in the heater and has a unit of watts, and $t_e = L_e^2/(2\alpha_s)$. Fushinobu *et al.* [5] concluded that equation (1) gives lower values of the local heater temperature rise compared with the numerical and experimental results for the entire frequency range. The constant $A = 1.14$ is thus introduced here to improve the fit with the numerical results. Equation (1) is nondimensionalized in the following form:

$$\theta_c = \Delta T_c \lambda_s L_e/Q = A\{(\sqrt{2\pi} + \sqrt{f/f_e})^2 + f/f_e\}^{-1/2}, \quad (2)$$

where

$$f/f_e = f\pi L_e^2/\alpha_s = (2Fo_s)^{-1}. \quad (3)$$

The frequency, $f_e = \alpha_s/(\pi L_e^2)$, represents a typical heating frequency below which ΔT_c can be approximated by its steady-state value and above which the approximation is no longer valid.

Convection-governed substrate temperature rise

Amplitude of the convection-governed substrate temperature rise, ΔT_s, is determined from the following relationship:

$$\rho_s c_s V_s \frac{dT_s(t)}{dt} = -hA_s\{T_s(t) - T_0\} + Q(t), \quad (4)$$

where ρ_s is the substrate density, c_s is the substrate specific heat, h is the heat transfer coefficient of the substrate cooling, $A_s = L_s^2$ is the upper surface area of the substrate, L_s is the substrate length, $V_s = A_s \times L_y$ is the substrate volume, L_y is the substrate thickness, $T_s(t)$ is the substrate temperature as a function of time, T_0 is the ambient temperature, and $Q(t)$ is the heat generation rate as a function of time. As shown in Fig. 1, the substrate temperature T_s is modeled to be lumped, i.e. uniform over the entire substrate. Equation (4) can be easily solved with heat generation rate $Q(t)Q\cos(2\pi ft)$. The solution $T_s(t) - T_0$ shows sinusoidal time dependence, and the amplitude of the solution,

$$\Delta T_s = Q\{(2\pi\rho_s c_s V_s f)^2 + (hA_s)^2\}^{-1/2} \quad (5)$$

is the desired substrate temperature rise. Equation (5) is nondimensionalized in the following form:

$$\theta_s = \Delta T_s \lambda_s L_e/Q = \{(2\gamma_y f/\gamma_e^3 f_e)^2 + (Bi_s/\gamma_e)^2\}^{-1/2}, \quad (6)$$

where $Bi_s = hL_s/\lambda_s$ is the Biot number, $\gamma_e = L_e/L_s$ is heater-substrate size ratio, and $\gamma_y = L_y/L_s$ is the substrate thickness-size ratio.

Finally, the nondimensional amplitude of the heater temperature rise θ_e is given as a combination of equations (2) and (6) as follows:

$$\theta_e = \theta_c + \theta_s. \quad (7)$$

Equation (7) gives the analytical values of the maximum heater temperature rise as a function of nondimensional heating frequency, convective cooling condition and size parameters.

Calculation of equation (7) requires an estimation of the Biot number, Bi_s, which requires the value of the average heat transfer coefficient of the upper substrate surface h. Since the boundary layer flow over a flat plate is considered in the present work, the local heat transfer coefficient that incorporates the unheated starting length of the velocity boundary layer [7] can be used,

$$h(x) = 0.332\lambda_f Pr^{1/3}(U_0/\nu x)^{1/2}\{1-(L_0/x)^{3/4}\}^{-1/3}, \quad (8)$$

where λ_f is the fluid thermal conductivity, x is the distance from the starting point of the velocity boundary layer, and L_0 is the unheated starting length of the velocity boundary layer. Integration of equation (8) over the entire substrate length from $x = L_0$ to $L_0 + L_s$, divided by the substrate thermal conductivity λ_s, gives the Biot number.

Due to the consistency with the following numerical calculations section, the heater is located on the substrate surface, and the heat transfer area, A_s, is defined as the upper surface area of the substrate. Note, however, that the present analysis allows the heater to be embedded in the substrate. This is due to the fact that θ_c is derived from the heat conduction equation in the substrate, and it is easily calculated when the heater is embedded. Once θ_c can be accurately modeled, equation (7) can be used in the heater temperature calculation. Another issue to be noted is that A_s can be any part of the substrate surface where h is defined. For instance, when many heaters are mounted on the substrate, the A_s of each individual heater effectively decreases proportional to the number of heaters. In these cases, the substrate surface area divided by the number of heaters can be used as A_s. These are the advantages of the present analysis when used in microelectronics applications, where many micro heat generating devices are fabricated on the semiconductor chips and sealed with plastic molds or other materials. With the appropriate modeling of θ_c and A_s, θ_e of the micro heat generating devices, such as transistors, can be estimated in a similar manner.

NUMERICAL CALCULATION

Figure 2 shows the computational domain of the numerical calculation. The computational domain consists of a substrate and the fluid flow. A heater, which is the only heat generating region heating

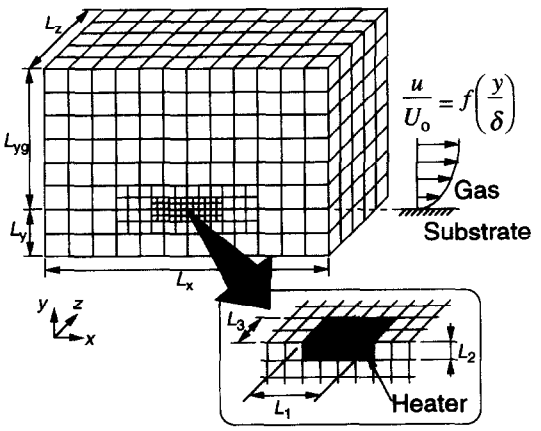

Fig. 2. A schematic of the three-dimensional computational domain. The domain consists of the fluid, substrate and the heating element.

element, exists on the substrate at the fluid–substrate interface. The heater size L_1 given in Fig. 2 corresponds to L_e and L_3 is $L_e/2$. Uniform heat generation is assumed in the heater. The velocity profile in the fluid flow is given by a similarity solution of the boundary layer flow on a flat plate. The detail is given in Nagasaki *et al.* [4].

The numerical calculation is based on the previous works [4, 5]. In the present work, however, the periodic steady-state temperature field in the solid substrate and fluid flow is obtained. The nondimensionalized energy equation,

$$\frac{1}{Fo_m}\frac{\partial\theta}{\partial\tau}+RePr\left\{\frac{\partial}{\partial\xi}(\tilde{u}\theta)+\frac{\partial}{\partial\eta}(\tilde{v}\theta)\right\}=\frac{\partial^2\theta}{\partial\xi^2}+\frac{\partial^2\theta}{\partial\eta^2}+\frac{\partial^2\theta}{\partial\zeta^2}+\sigma \quad (9)$$

is solved numerically in the fluid and substrate, respectively. In the equation, Fo_m is the Fourier number, θ is the nondimensional temperature rise as a function of time and position, τ is the nondimensional time, Re is the Reynolds number, Pr is the Prandtl number, ξ, η and ζ are the nondimensionalized coordinates, $\tilde{u}$ and $\tilde{v}$ are the nondimensionalized velocities, and σ is the nondimensional heat generation rate per unit volume as a function of time and position. The suffix 'm' denotes either 'f' (fluid) or 's' (substrate). Since the heat generation occurs only in the heater, the heat generation term σ has a finite and uniform value in the heater and is zero the rest of the substrate and the fluid. The nondimensional fluid velocities $\tilde{u}$ and $\tilde{v}$ are zero in the substrate. Nondimensionalization follows the previous works, however, some of the definitions are given below for further discussions:

$$Fo_m=\alpha_m/(2\pi fL_e^2) \quad (10a)$$

$$Re=U_0L_e/\nu \quad (10b)$$

$$\theta=(T-T_0)\lambda_sL_e/Q \quad (10c)$$

where α_m is the thermal diffusivity of either the fluid (α_f) or the substrate (α_s), f is the heating frequency, L_e is the heater size, U_0 is the bulk fluid velocity, ν is the fluid kinematic viscosity, T is the dimensional temperature as a function of time and position, T_0 is the ambient temperature, and λ_s is the substrate thermal conductivity.

The heater-substrate size ratio, γ_s, does not explicitly appear in the derivation of the governing equation, although it is the major parameter that governs the heater temperature rise. The parameter determines the nondimension substrate size. It is therefore expected that γ_e predominantly governs the heater temperature rise through the heat capacity of the substrate and the effect of the boundary conditions.

Equation (9) is solved numerically under sinusoidal periodic steady-state heat input in the heater. The complex temperature, $\theta^c=\theta_a^c\exp(i\tau)=\theta+i\theta'$, is therefore introduced [5] to reduce the computation time, where the real part corresponds to the nondimensional temperature in equation (9). Details of the derivation are given in Fushinobu *et al.* [5]. Note that the calculated heater temperature rise is a sinusoidal function of the time. However, only its amplitude, θ_e, is presented and compared with the analytical results in the following discussions, because the amplitude is the major concern in most applications.

A domain decomposition technique is employed in order to accurately predict the temperature field at small length scales in a large computational domain. An adiabatic boundary condition is applied at all the surfaces except for the in-flow and out-flow boundaries of gas. The details of the numerical calculation are given in elsewhere [4, 5].

RESULTS AND DISCUSSIONS

Comparison between the modeled analysis and the numerical calculation

Figure 3 shows the comparison between the analytical model and the numerical calculation. The horizontal axis denotes the nondimensional heating frequency f/f_e and is equal to a half of the inverse of the substrate Fourier number, $1/(2Fo_s)$, from its defi-

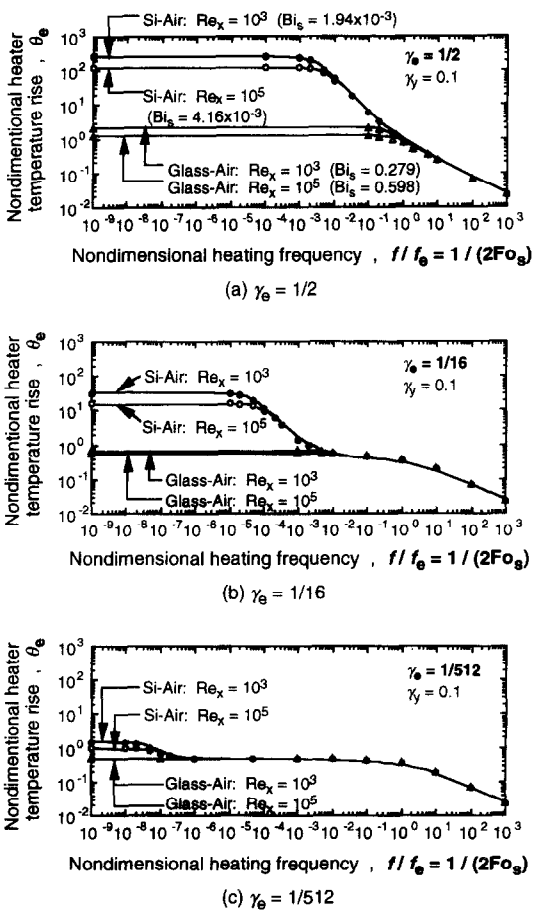

Fig. 3. Calculated nondimensional heater temperature rise θ_e as a function of nondimensional heating frequency f/f_e.

nition. The range of f/f_e in Fig. 3(a), for instance, corresponds up to $f = 73$ MHz, which covers the operation frequency of most of the silicon based devices, for a 20 μm heat generating device on a 1 cm silicon chip. The vertical axis is the amplitude of the nondimensional heater temperature rise θ_e. The results are compared under various conditions: two different substrate materials (Si and Glass), two Reynolds numbers ($Re_x = 10^3, 10^5$), and three heater-substrate size ratios ($\gamma_e = L_e/L_s = 1/2, 1/16, 1/512$). The corresponding Biot numbers are given in Fig. 3(a). The solid lines represent the modeled analytical solution and the symbols denote the rigorous numerical results. The circular and the triangular symbols denote the silicon substrate and the glass substrate case, respectively.

The definition of the Reynolds number, Re_x, used here is different from equation (10b), where the heater size L_e is used for characteristic length. It is

$$Re_x = U_0 x_e/\nu, \tag{11}$$

where x_e is the distance between the beginning of the boundary layer to the center of the heater. The values of the Reynolds number, $Re_x = 10^3$ and 10^5, in Fig. 3 confirm the laminar air flow. The values, $Re_x = 10^3$ and 10^5, correspond to the following values of previously defined Reynolds number at each heater-substrate size ratio: $Re = 290$ and 2900 at $\gamma_e = 1/2$, $Re = 36$ and 360 at $\gamma_e = 1/16$, and $Re = 1.1$ and 11 at $\gamma_e = 1/512$. These Reynolds numbers correspond to $U_0 = 0.8 \sim 8$ m s^{-1} when air is flowing over the 1 cm length substrate.

The comparison between the numerical and analytical results gives excellent agreement over the entire frequency range, despite the rough approximation of the modeled temperature. Although the maximum relative error of the analytical results to the numerical results reaches 25% at $f/f_e = 1$ in Fig. 3(a), 23% at $f/f_e = 5 \times 10^{-3}$ in Fig. 3(b), and 19% at $f/f_e = 10^{-7}$ in Fig. 3(c) on 'Si–Air: $Re_x = 10^3$', the relative errors are within $\pm 10\%$ in general. This agreement suggests that the simple analytical model is a good substitute for the rigorous numerical calculation.

The results show interesting features. First, especially in the case of the silicon substrate with $\gamma_e \leqslant 1/16$, θ_e reaches a constant value to form a plateau region with decreasing f/f_e; however, it again starts to increase and forms another plateau. These two plateau regions can be explained by the penetration depth of the heat conduction for periodic heating case $L_{th} = (\alpha_s t^*)^{1/2}$, where $t^* = 1/(2\pi f)$ is the characteristic heating time scale. The penetration depth, L_{th}, which is equal to $(Fo_s)^{1/2} L_e$ from its definition, reaches about seven times longer than the heater size ($L_{th} = 7.1 \times L_e$) when the nondimensional heating frequency, $f/f_e = 1/(2Fo_s)$, is equal to 10^{-2} for instance. Apparently it exceeds the heater size and the temperature profile at the heater size length scale can be regarded as reaching its steady-state profile. However, the substrate size is larger than the penetration depth, and the temperature profile at the substrate size length scale can rise with increasing the characteristic heating time scale. It can thus be explained that the first constant value is a constant value for the local heater temperature rise, θ_0, and the final constant value is for the substrate temperature rise, θ_s.

Secondly, the value of the second plateau region, which appears at lower heating frequency, drastically varies with changing the parameters. For example, the highest value ($\theta_e = 2.52 \times 10^2$) in Fig. 3(a) is more than 500 times bigger than the smallest value in Fig. 3(c). Comparison of the figures show that θ_e decreases with the increasing Bi_s and the decreasing γ_e. Since the local heater temperature rise θ_c is a function of only f/f_e, as shown in equation (2), the variation of θ_e is attributed to the substrate temperature rise θ_s that is governed by the convection heat transfer. Note also that the local heater temperature rise at $f/f_e = 0$, $\theta_c = 0.455$, cannot be neglected compared with the substrate temperature rise, $\theta_s = \theta_e - \theta_c = 0.955$, when Si–Air, $Re_x = 10^5$, and $\gamma_e = 1/512$. This comparison suggests that the temperature of small electronic devices in ICs can be much higher than the chip bulk temperature, and that the rigorous device temperature estimation requires the device level heat transfer characteristics.

Regime map for convective cooling of a small heater on a substrate

Discussions on Fig. 3 revealed two important issues that govern the heater temperature rise, namely, (a) whether the convection-governed substrate heater temperature rise dominates the heater temperature or the conduction-governed local heater temperature rise does, and (b) whether or not θ_c and θ_s reach their steady-state values. These conditions reduce to the following criteria:

θ_c is negligible compared with θ_s when

$$\theta_c = 0.1 \times \theta_s \tag{12a}$$

θ_s is negligible compared with θ_c when

$$\theta_s = 0.1 \times \theta_c \tag{12b}$$

θ_c reaches a constant value when

$$\theta_c = 0.9 \times \theta_{c0} \tag{12c}$$

θ_s reaches a constant value when

$$\theta_s = 0.9 \times \theta_{s0}. \tag{12d}$$

Here, 10% is chosen to be the critical value. The constants θ_{c0} and θ_{s0} represent the values of θ_c and θ_s at $f/f_e = 0$, respectively. Equation (12a–d) can be easily calculated with equations (2) and (6), and give the

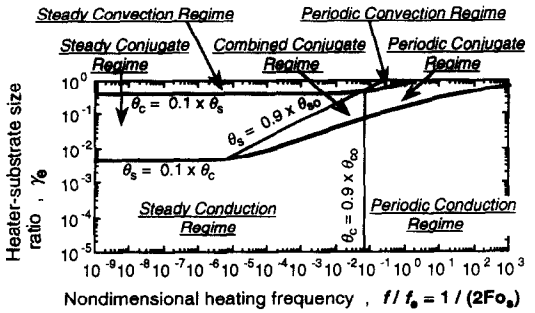

Fig. 4. Typical regime map for heater temperature prediction ($Bi_s = 0.1$, $\gamma_y = 0.1$).

heat transfer regime map shown in Fig. 4. The horizontal axis is the nondimensional heating frequency f/f_e, and the vertical axis is the heater-substrate size ratio γ_e. Since the regime map is constructed based on equations (2) and (6), the map varies with two key parameters in the equations; the Biot number, Bi_s, and the substrate thickness-length ratio $\gamma_y = L_y/L_s$. Arbitrary values are chosen here to be $Bi_s = 0.1$ and $\gamma_y = 0.1$ to discuss the general behavior.

Firstly, Fig. 4 shows the governing heat transfer mode that determines the heater temperature rise. Below the line named '$\theta_s = 0.1 \times \theta_c$', θ_s can be neglected compared with θ_c, while θ_c can be neglected compared with θ_s above the line named '$\theta_c = 0.1 \times \theta_s$'. The conjugate conduction and convection heat transfer nature of the problem must be considered in the regime between the two lines. Note that the convection effect does not appear $\gamma_e < 4.6 \times 10^{-3}$ regardless of f/f_e. Since the substrate temperature rise is negligibly smaller than the local heater temperature rise in this regime, the convection effect on the heater temperature, which appears through the substrate temperature change, is also negligible. Also the governing heat transfer mode varies with increasing heating frequency, even if the heater-substrate size ratio is constant.

Secondly, Fig. 4 shows the heater temperature should be determined from either a periodic steady-state governing equation or a steady-state equation. Here the periodic steady-state governing equation means the time-dependent energy equation, such as equation (9), with periodic heating term, and the steady-state equation means the energy equation without any time-dependent term. When f/f_e is smaller than the lines named '$\theta_s = 0.9 \times \theta_{s0}$' and '$\theta_c = 0.9 \times \theta_{c0}$', and θ_c can be regarded as constant values, respectively. Thus, $\theta_e = \theta_c + \theta_s$ is constant when f/f_e is smaller than the line of '$\theta_s = 0.9 \times \theta_{s0}$', and the steady-state governing equation can be used to evaluate the heater temperature. On the other hand, both θ_c and θ_s depend on the heating frequency when f/f_e is bigger than the line of '$\theta_e = 0.9 \times \theta_{c0}$', and the periodic steady-state governing equation must be used. The periodic steady-state substrate temperature rise and the steady-state heater local temperature rise should be combined in the regime between the two lines.

Based on the above discussions, the regime map is divided into the following seven regimes; the periodic steady-state conduction-governed heater local temperature rise is dominant in the 'periodic conduction regime', the steady-state heater local temperature rise in the 'steady conduction regime', the periodic steady-state convection-governed substrate temperature rise in the 'periodic convection regime', and the steady-state substrate temperature rise in the 'steady convection regime'. Steady-state temperature rise of both the heater local and the substrate is important in the 'steady conjugate regime', periodic steady-state temperature rise of both the heater local and the substrate in the 'periodic conjugate regime', and the steady-state heater local temperature rise and the periodic steady-state substrate temperature rise should be combined to give θ_e in the 'combined conjugate regime.'

Figure 5 shows the regime map for the parameters used in the present numerical calculations. The solid lines denote the limit for steady-state temperature, and the thicker solid lines denote the governing heat transfer mode. The dashed lines are plotted to show the value of $\gamma_e = 1/512$ for the following discussions. The differences in Fig. 5(a–d) basically reside in the change of Bi_s from 1.94×10^{-3} to 0.598.

Figure 5(a) and (b) are regime maps for the silicon substrate cases. Although the lines of '$\theta_s = 0.1 \times \theta_c$' do not show constant values of γ_e at lower frequencies in the figures, they reach constant values of $\gamma_e = 8.9 \times 10^{-5}$ at $f/f_e < 10^{-11}$ for Fig. 5(a) and $\gamma_e = 1.9 \times 10^{-4}$ at $f/f_e < 10^{-10}$ for Fig. 5(b). It can be seen in Fig. 5(a) that the governing heat transfer characteristics changes with f/f_e at constant γ_e. At $\gamma_e = 1/512$, the heater temperature is in the 'periodic conduction regime' above $f/f_e = 7 \times 10^{-2}$, 'steady conduction regime' below $f/f_e = 7 \times 10^{-2}$, 'combined conjugate regime' below $f/f_e = 7 \times 10^{-7}$, and 'steady conjugate regime' below $f/f_e = 1.5 \times 10^{-8}$. These values correspond to the frequency-dependent behavior of the curve in Fig. 3(c). It can be also seen from these figures that the heater temperature rise θ_e can actually be well predicted by ignoring the local heater temperature rise θ_c above the '$\theta_c = 0.1 \times \theta_s$' line. For instance, the temperature rise of steady-operation electronic devices bigger than 200 μm^2 on a 1 cm^2 silicon chip is nearly equal to the bulk chip temperature rise. This means that the thermal design of the chip does not require device level consideration. However, the device level consideration becomes important below the line; the local temperature rise can become far above the chip bulk temperature rise for devices typically smaller than 1 μm^2. For example, transistors with 1 mW heat generation rate and 0.5 μm characteristic dimension give more than 5 K local temperature rise.

Comparison between Fig. 5(a) and (b) shows that the 'steady convection regime' becomes smaller when the Biot number is increased. This is due to the

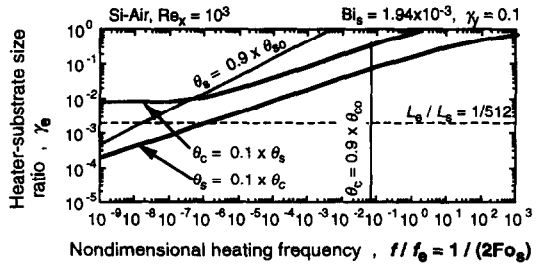

(a) Si-Air: $Re_x = 10^3$ ($Bi_s = 1.94 \times 10^{-3}$)

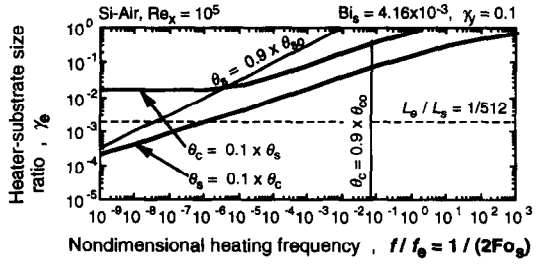

(b) Si-Air: $Re_x = 10^5$ ($Bi_s = 4.16 \times 10^{-3}$)

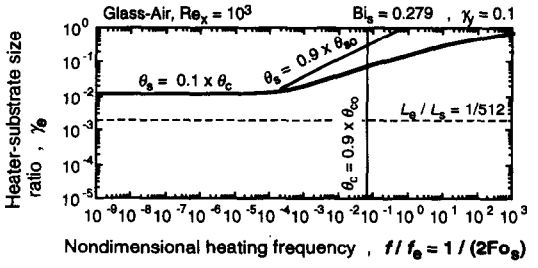

(c) Glass-Air: $Re_x = 10^3$ ($Bi_s = 0.279$)

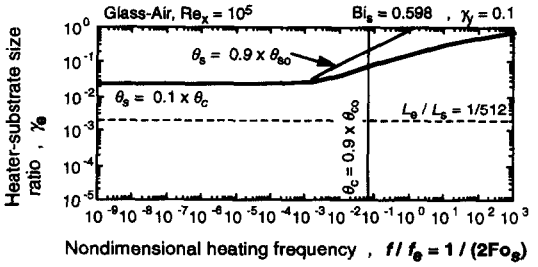

(d) Glass-Air: $Re_x = 10^5$ ($Bi_s = 0.598$)

Fig. 5. Regime map for calculated results in the present work ($\gamma_y = 0.1$).

decrease of θ_s with the enhanced heat transfer and resulting relative increase of the contribution of θ_c in θ_e. This trend is important when cooling fins, boiling, or other advanced cooling techniques are used; θ_e may considerably differ from θ_s.

Figure 5(c, d) shows the regime maps for the glass substrate cases. The 'steady convection regime' and the 'periodic convection regime' disappear in these figures. Moreover, although the governing heat transfer characteristics changes as discussed in Fig. 5(a), θ_s never becomes significant in Fig. 5(c, d) at $\gamma_e = 1/512$. These trends are due to the poor thermal conductivity of the glass substrate. Figure 3(c) confirms this result, where θ_e at lower f/f_c is nearly equal to θ_c and thus, θ_s is negligible.

CONCLUSIONS

A new, simple, and easy to use analytical model that predicts the general behavior of the temperature rise of a small heater mounted on an unheated substrate and cooled by a surrounding fluid is developed. The model results give excellent agreement with rigorous numerical calculations. The model is used to construct a regime map that predicts the heat transfer characteristics of the small heater. The map suggests proper modeling of the thermal design of electronic devices depending on the given parameters.

Acknowledgements—This work is supported by a grant-in-aid for Developmental Scientific Research (no. 01850047) from the Ministry of Education in Japan. KF acknowledges the help of the Japan Society for the Promotion of Science. The authors thank L. M. Phinney, J. P. Longtin, and C. H. Goldman at University of California, Berkeley for their help.

REFERENCES

1. A. Zabib and Y. K. Wo, A two-dimensional conjugate heat transfer model for forced air cooling of an electronic devices, *ASME J. Electron. Packaging* **111**, 41–45 (1989).
2. D. E. Wroblewski and Y. Joshi, Computations of liquid cooling for a protruding heat source in a cubical enclosures, *Int. J. Heat Mass Transfer* **36**, 1201–1218 (1993).
3. K. Hijikata, W. Nakayama, T. Nagasaki, R. Kurazume and K. Fushinobu, A study on heat transfer from small heating elements in an integrated circuit chip, *Proc. of the ASME/JSME Thermal Engineering Joint Conf.*, Reno, NV, Vol. 4, pp. 93–98 (1991).
4. T. Nagasaki, K. Hijikata, K. Fushinobu and P. E. Phelan, Numerical simulation of the conjugate direct cooling of a micro heat generating element, *Proc. of* 1992 *Joint ASME/JSME Conf. on Electronic Packaging*, Milpitas, CA, Vol. 1, pp. 217–223 (1992).
5. K. Fushinobu, P. E. Phelan, T. Nagasaki, K. Hijikata and M. I. Flik, *Periodic Steady-State Thermal Analysis of a High-*T_c *Superconducting Microbolometer*, HTD-Vol. 200, pp. 89–95. ASME (1992).
6. T.-L. Hwang, S. E. Schwarz and D. B. Rutledge, Microbolometers for infrared detection, *Appl. Phys. Lett.* **180**, 251–258 (1979).
7. E. R. G. Eckert, *Heat and Mass Transfer*, pp. 173–178. McGraw-Hill, New York (1959).